ACS SENSORS

pubs.acs.org/acssensors

Article

Polarimetric Balanced Detection: Background-Free Mid-IR Evanescent Field Laser Spectroscopy for Low-Noise, Long-term Stable Chemical Sensing

Stephan Freitag,[§] Matthias Baer,[§] Laura Buntzoll, Georg Ramer, Andreas Schwaighofer, Bernhard Schmauss, and Bernhard Lendl*

Cite This: *ACS Sens.* 2021, 6, 35−42

Read Online

ACCESS | Metrics & More | Article Recommendations

ABSTRACT: In this work, we introduce polarimetric balanced detection as a new attenuated total reflection (ATR) infrared (IR) sensing scheme, leveraging unequal effective thicknesses achieved with laser light of different polarizations. We combined a monolithic widely tunable Vernier quantum cascade laser (QCL-XT) and a multibounce ATR IR spectroscopy setup for analysis of liquids in a process analytical setting. Polarimetric balanced detection enables simultaneous recording of background and sample spectra, significantly reducing long-term drifts. The root-mean-square noise could be improved by a factor of 10 in a long-term experiment, compared to conventional absorbance measurements obtained via the single-ended optical channel. The sensing performance of the device was further evaluated by on-site measurements of ethanol in water, leading to an improved limit of detection (LOD) achieved with polarimetric balanced detection. Sequential injection analysis was employed for automated injection of samples into a custom-built ATR flow cell mounted above a zinc sulfide multibounce ATR element. The QCL-XT posed to be suitable for mid-IR-based sensing in liquids due to its wide tunability. Polarimetric balanced detection proved to enhance the robustness and long-term stability of the sensing device, along with improving the LOD by a factor of 5. This demonstrates the potential for new polarimetric QCL-based ATR mid-IR sensing schemes for in-field measurements or process monitoring usually prone to a multitude of interferences.

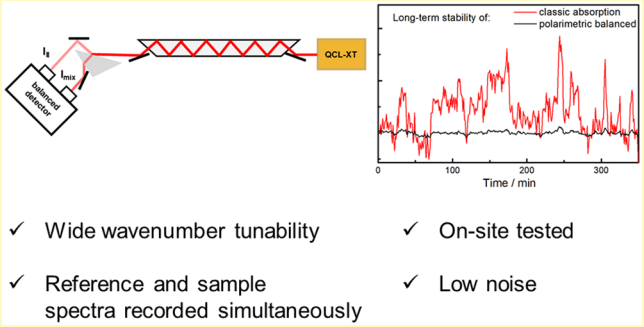

KEYWORDS: *mid-infrared spectroscopy, attenuated total reflection, quantum cascade lasers, balanced detection, process analytical technology*

Infrared (IR) spectroscopy is a powerful analytical technique based on probing molecular vibrations in a rapid and label-free manner.[1] It has been employed for sensing applications in gases[2,3] and liquids.[4,5] Due to its robustness and ease of operation, attenuated total reflection (ATR) IR spectroscopy found its way into process analytics[4,6] and in-field applications.[5,7] In this technique, light is totally reflected in the optical denser ATR element, generating an evanescent field penetrating into the (optically less dense) sample placed on top of the element, typically up to 2 μm.[8] Fourier transform (FT) IR spectrometers are considered the gold standard in IR spectroscopy. Combined with ATR settings, they are employed in process analytics,[6] clinical chemistry,[9] to study complex catalytic reactions,[10] forensic science,[11] and material identification[12] among other applications. In conventional ATR IR absorption spectroscopy approaches, e.g., in process monitoring, a background spectrum needs to be recorded at a certain point in time, usually prior to the sample measurements, which are recorded over a longer period of time. However, along this time period, there may occur diverse incidents (e.g., ATR element fouling, drifts of environmental parameters), which lead to artifacts in the resulting absorbance spectra and impair successful analysis.

Developments in the last two decades based on a new powerful mid-IR radiation source, so-called quantum cascade lasers (QCLs), lead to devices that challenge FT-IR spectrometers regarding their performance.[13] In addition to their higher brightness, QCLs also offer coherent and linear polarized light. The latter feature was exploited for QCL-based vibrational circular dichroism,[14] the characterization of

Received: July 2, 2020
Accepted: December 11, 2020
Published: December 29, 2020

https://dx.doi.org/10.1021/acssensors.0c01342
ACS Sens. 2021, 6, 35−42

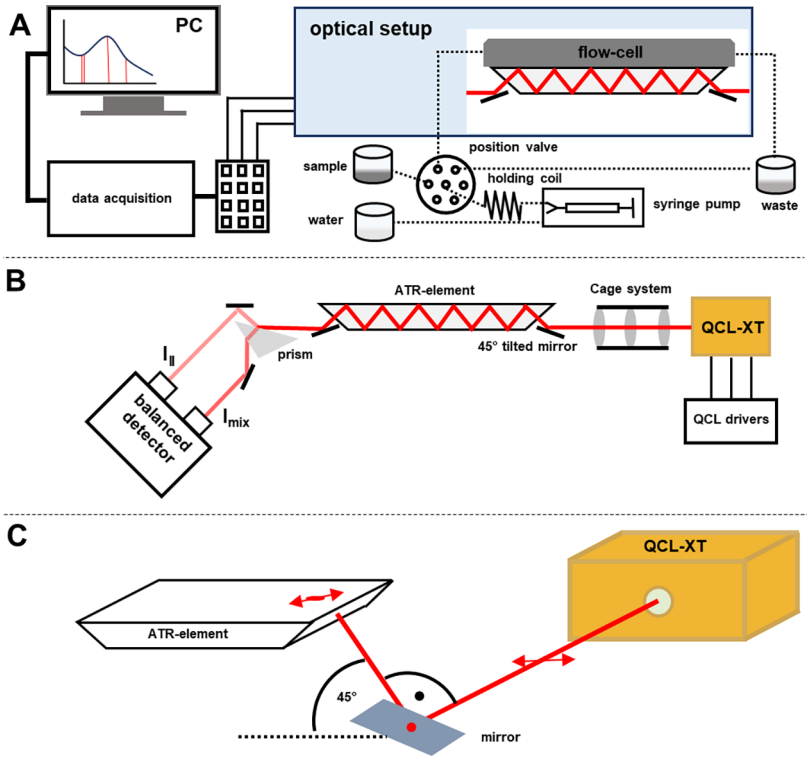

Figure 1. (A) Scheme of the entire experimental setting, consisting of optics, liquid handling, and data acquisition. (B) Scheme of the optical setup, ATR element shown in the side view. (C) Scheme of 45° tilt of the incident infrared beam to shift polarization in respect to the ATR-element surface.

anisotropic materials via atomic force microscopy-infrared spectroscopy,[15] and rapid mid-IR ellipsometry.[16,17] Nowadays, distributed feedback (DFB)-QCLs and external cavity (EC)-QCLs are the most commonly employed mid-IR laser types. DFB-QCLs emit in a very narrow range and are thus employed for gas-phase analysis, whereas EC-QCLs provide broad spectral coverage, hence being suitable for sensing in liquids.[18−20] EC-QCLs rely on movable diffraction gratings for tuning over a broad spectral range. As a consequence, these lasers are fairly bulky and often prone to mode-hopping during tuning, originating from competing optical modes, which results in laser noise.[21,22] Dedicated signal processing schemes and mode tracking systems have been employed to counter this drawback.[21] In contrast to EC-QCLs, a new tuning mechanism based on the Vernier effect for eXTended tunable QCLs was reported (QCL-XT).[23] These widely tunable devices are monolithic like DFB-QCLs, hence no movable parts are involved. Tuning to the desired wavelength is achieved by heating one of two integrated superstructure grating sections on top of the laser element.[24,25] QCLs have also been utilized for building evanescent field absorption-based sensors using waveguides.[2,26] The combination of ATR with EC-QCLs for biomedical applications and surface-modified ATR elements for signal enhancement has been reported recently.[27−29] Besides their advantages, QCLs show significant noise compared to classic thermal emitters.[21] This laser noise is a well-known problem of high-intensity light sources and has been tackled even before the appearance of QCLs with optical feedback stabilization or balanced detection.[30] In the latter technique, laser radiation is split and directed on two detectors, thus the additional detector is used as a reference. This design allowed to cancel out not only laser noise but also interference from other sources.[30] Creative sensor design in QCL-based photothermal spectroscopy showed significant noise reduction by employing balanced detection for the probe laser.[31] For mid-IR laser-based transmission spectroscopy, an EC-QCL setup was introduced compensating for QCL intensity noise, employing balanced detection via two liquid-nitrogen-cooled mercury cadmium telluride (MCT) detectors;[32] more recently, an EC-QCL setup incorporating a dual-channel transmission cell paired with a dedicated thermoelectrically cooled balanced detection setup was reported.[33]

In this work, we introduce a novel approach to reduce noise in a QCL-based ATR sensing scheme via polarimetric balanced detection. Exploiting the difference in sensitivity experienced by two laser beams of different polarization allows for simultaneous recording of the background and sample spectra. We combined a multibounce ATR setup with a widely tunable monolithic QCL-XT and a dedicated thermoelectrically cooled balanced MCT detection module. The sensor was placed in a water treatment plant, utilizing the noise suppression capabilities of polarimetric balanced detection to showcase the advantages for on-site operation. For demonstration purposes, we measured ethanol in water at different concentrations, showing the suitability of QCL-XTs for liquid sensing. We observed different absorbance values depending on the IR beam polarization and displayed the advantages of polarimetric balanced detection.

To the best of our knowledge, this is the first report of polarimetric-based balanced detection in combination with QCL-XT for liquid sensing using ATR IR spectroscopy.

EXPERIMENTAL SECTION

Experimental Setup. The experimental setup is shown in Figure 1.

https://dx.doi.org/10.1021/acssensors.0c01342
ACS Sens. 2021, 6, 35−42

Table 1. QCL-XT Settings for Tuning to the Chosen Wavenumbers

	1265.43 cm^{-1}	1273.5 cm^{-1}	1289.68 cm^{-1}	1292.33 cm^{-1}
T [°C]	40	40	40	40
I_{laser} [mA]	564	564	900	564
$I_{front\ heater}$ [mA]	0	0	752	690
$I_{back\ heater}$ [mA]	622	0	0	0

For polarimetric balanced detection ATR experiments, the device was placed in the surveillance room of a water treatment plant in Genova.[34] Due to the harsh environment, such as room-temperature fluctuations due to poor isolation and vibrations originating from operating pumps and voluminous pipes with flowing water, the optical setup was wrapped by a thermal insulating housing linked to a custom-built water-cooling system. Silica gel (1 kg) was used as a drying agent to stabilize humidity and placed in the housing to counter interferences caused by water vapor. A TSP01 USB Temperature and Humidity Data Logger (Thorlabs, New Jersey) was used for monitoring environmental parameters. The IR beam emitted by the QCL-XT (Alpes Lasers, Neuchatel, Switzerland) was guided into a multibounce zinc sulfide (ZnS) ATR element (17 × 10 × 1 mm^3, 45°) purchased from Crystran (Poole, United Kingdom). The ATR element geometry would allow for eight bounces, however only five bounces are accessible due to the flow cell geometry. An ATR fixture holding the element was designed in-house and manufactured using 3D-printing.[5,35] After assembling the optical setup, the flow cell housing a sample compartment with a volume of approximately 20 μL (see Figure 1A) was placed on top of the ATR element and sealed by an O ring. The cell was milled out of aluminum by Protolabs (Feldkirchen, Germany), following self-drawn blueprints. Due to its transparency, the ZnS ATR element allowed for elegant adjustment of the optics using an auxiliary red laser. Fine adjustment of the optics was done by operating the QCL-XT at 1273.5 cm^{-1} and monitoring the signal at the detectors using an oscilloscope. Care was taken to avoid fringes observed in the signal of both optical channels as well as to maximize the signal at the detector and simultaneously avoiding detector saturation by application of the described cage system. After completing the assembly of the experimental setup, the housing was closed and the flow cell filled with water. Sample injection and washing in-between the experiments were done by a sequential injection system,[36] involving a syringe pump equipped with a 100 μL syringe paired with a position valve supplied from Hamilton (Bonaduz, Switzerland). Teflon tubings (1/16-inch) with the inner diameter of 0.18 mm (VICI, Schenkon, Switzerland) were used to connect the liquid reservoirs, the syringe pump, and the position valve as well as to wind the holding coil. The sequential injection system was controlled via a custom-made java-based program (A.U.G. Signals Hellas, Athens, Greece). Ethanol (95%) was purchased from Sigma-Aldrich (Steinheim, Germany) and diluted to the desired concentration using distilled water. The IR beam emitted by the QCL-XT was directed through a cage system featuring a lens for beam expansion, an aperture for attenuation to avoid detector saturation, and followed by a lens for refocusing of the beam. To make use of polarization-dependent absorption, evanescent waves of both polarizations have to be excited at the ATR junction. The laser itself emits horizontally polarized light. As outlined in Figure 1C, a mirror was mounted in a way that the reflected laser beam propagates perpendicular to the incident laser beam but is also directed upward by an angle of 45° in respect to the ground plane. The redirected beam then hits the entrance facet of the ATR element. This arrangement has the advantage that in respect to the sample-active ATR surface, the polarization is neither purely parallel (p) nor purely perpendicular but has equal components of both polarizations. After sample interaction, the beam was directed toward a zinc selenide (ZnSe) prism mounted in the Brewster angle, which acts as a polarizer. This allows the separation of the incident beam into two beams composed of different polarizations. The reflected beam contained purely p-polarized radiation in respect to the ATR surface and a transmitted beam of mixed polarization, mainly containing perpendicular-polarized light. A prism as a polarizing element offers the advantage that it has no parallel surfaces and thus no optical resonances (fringes) are introduced. For polarization separation, the optical setting (prism and mirrors) was designed in a way that both beams experience the same optical path length. Thus, also the focal points of both optical paths lie in the same plane, i.e., the position of the two active elements of the balanced detection module (Vigo Systems, Warsaw, Poland). This module was custom made and combines in one housing two thermoelectrically cooled MCT detector elements optimally matched regarding their transimpedance, voltage responsivity, and detectivity.[33] Data acquisition was performed via a USB-6281 Multifunction I/O Device linked to a BNC-2110 connector block (National Instruments, Houston) connected to a PC using a 25 kHz sampling rate. Data recording and laser control were performed using MATLAB (Mathworks, Massachusetts). Three S2 gen5 laser drivers (Alpes Lasers, Neuchatel, Switzerland) were used to control the QCL-XT, allowing for tuning the lasers to the chosen wavenumbers (one to drive the laser emission, two for heating front and back mirrors, Table 1).[23] The laser was operated at a 100 Hz pulse rate with a duty cycle of 50%. The signals of the balanced detector module shown in Figure 2 were

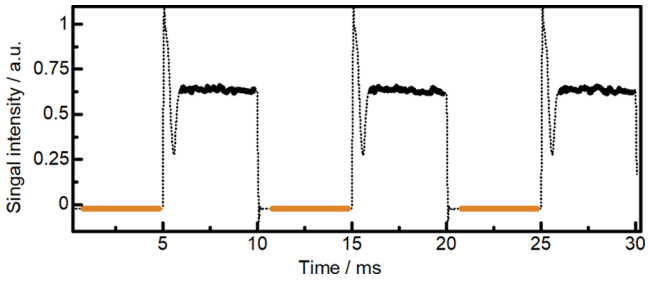

Figure 2. Recorded signal of one channel of the balanced detection module (black dotted line). Intervals used in the digital boxcar detection scheme for offset compensation (solid brown line). Signal intervals used for averaging (solid black line).

evaluated using a digital boxcar detection scheme. For this purpose, a script was devised to perform the evaluation of the signal in four steps. First, synchronization was achieved by finding the falling edges of the signal. Second, the intervals of the signal where the laser was off (Figure 2, brown line) were averaged to give the detector offset. Third, intervals at which the laser was on and the signal was stable were selected (Figure 2, black line) and averaged. Fourth, the offset was subtracted from the averaged black marked intervals. Thus, it was possible to neglect the overshot at the rising edges of the signal. For the present work, the two single-ended detector signals were used, and hence polarimetric balancing was performed digitally. Tuning to a specific operation point takes less than a second. However, due to the change of the power dissipation, the temperature control of the laser takes some time to again stabilize the temperature to the nominal value. In total, the change of the emission wavenumber takes approximately 10−15 s.

Theoretical Considerations. In ATR spectroscopy, the extension of the evanescent field in the optically rarer medium can be described via the depth of penetration (d_p),[8,37]

$$d_p = \frac{\lambda_0}{2\pi\sqrt{n_1^2 \sin^2(\theta) - n_2^2}} \quad (1)$$

https://dx.doi.org/10.1021/acssensors.0c01342
ACS Sens. 2021, 6, 35−42

where λ_0 is the wavelength, n_1 and n_2 are the refractive indices of the ATR element as well as the sample, respectively, and θ is the angle of incidence. However, the depth of penetration, as shown in eq 1, is generally used as a measure of how far the electric field of the evanescent wave expanses into the optically rare medium before it decays to $1/e$.[37]

While the depth of penetration is independent of the polarization, the sensitivity for sample absorption is not. Here, a linear approximation of the absorption sensitivity is used, called effective thickness d_e. This parameter corresponds to the path length of a transmission setup that would exhibit the same absorption.[8,37] The expressions $d_{e,\perp}$ for perpendicular-polarized light, $d_{e,\parallel}$ for the parallel polarization, and d_e as the average of parallel and perpendicular light are[8]

$$d_{e,\perp} = N\frac{\lambda_0}{n_1}\cdot\frac{n_{21}\cos(\theta)}{\pi(1-n_{21}^2)[\sin^2(\theta)-n_{21}^2]^{1/2}} \quad (2)$$

$$d_{e,\parallel} = N\frac{\lambda_0}{n_1}\cdot\frac{n_{21}\cos(\theta)[2\sin^2(\theta)-n_{21}^2]}{\pi(1-n_{21}^2)[(1+n_{21}^2)\sin^2(\theta)-n_{21}^2][\sin^2(\theta)-n_{21}^2]^{1/2}} \quad (3)$$

$$d_e = N\frac{d_{e,\perp}+d_{e,\parallel}}{2} \quad (4)$$

For the employed experimental setup, N is the number of accessible reflections ($N = 5$) of the multibounce ATR element and n_1 and n_2 are the refractive indices for the ATR element and the probed liquid, respectively, ($n_{ij} = n_i/n_j$). For zinc sulfide $n_1 = 2.223$[38] and water $n_2 = 1.291$,[39] $\theta = 45$ and $\lambda_0 = 7.855$ μm; eqs 2−4 yield 8.63 μm for $d_{e,\perp}$, 26.30 μm for $d_{e,\parallel}$, and 17.47 μm for d_e.

FT-IR Measurements. FT-IR reference spectra were recorded with a Vertex 70v spectrometer (Bruker Optics, Ettlingen, Germany) equipped with a single-bounce Platinum ATR accessory (Bruker Optics, Ettlingen, Germany). Prior to spectrum acquisition, the spectrometer was evacuated and the sample compartment was flushed with dry air. A spectral resolution of 4 cm^{-1} was set for recording spectra in a double-sided acquisition mode. One hundred twenty eight scans were averaged per spectrum (acquisition time: 28.4 s) and calculated using a Blackmann-Harris 3-term apodization function and a zero-filling factor of 2. All spectra were acquired at room temperature. The aperture was set to 8 mm for maximum throughput. Ethanol in water mixtures (25 and 50%$_{vol}$) were used for recording reference spectra. Distilled water was used as a background. Spectra were analyzed using the software package OPUS 8.2 (Bruker Optics, Ettlingen, Germany).

RESULTS AND DISCUSSION

Sensor Stability and Operation. Directly after closing the housing of the optical setup, the water-cooling system, the QCL-XT, and the detectors were turned on, and temperature and humidity measurements were performed every 5 s for the duration of several hours. Figure 3A shows that after closing, the setup needs approx. 15 min for thermal stabilization. The depicted data also underlines the robustness of the thermal management system as the temperature after initial stabilization of the system does not exceed a standard variation of 15 mK. The increase in humidity after 300 min is linked to the limited resolution of the humidity sensor (see Figure 3A, dotted line). Simultaneously, also the signal from the two detector elements embedded into the balanced detection module was recorded (see Figure 3B). The difference in the signal intensity is explained by the unequal split of the beam at the prism used as the polarizer (see Figure 1B).

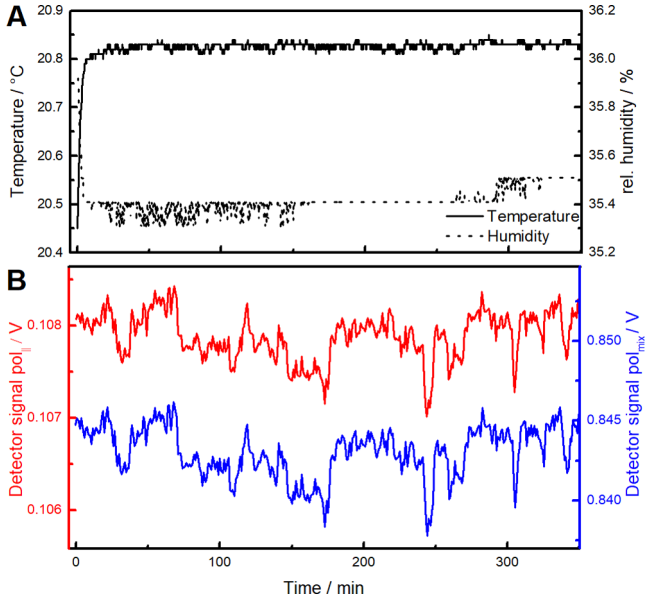

Figure 3. Long-term stability of the setup. (A) Temperature (solid line) and relative humidity (dotted line) in the setup. (B) Signal intensity for the two single-ended channels over time. The intensity of the mixed-polarized (blue) and parallel-polarized channels (red). The unequal intensity detected at the two channels is linked to the unequal split at the prism.

Polarimetric Balanced Detection. Classic IR absorption measurements for process monitoring use a background spectrum (I_0) recorded at a discrete point in time for comparison with continuously recorded sample spectra ($I_{(t)}$). Consequently, the obtained absorbance not only contains spectral information originating from analytes but also artifacts linked to various drifts over time, which adds noise. Figure 3B shows the recorded single-ended detector signals of both optical channels over several hours. Both signals feature significant noise, which scales with their intensities. These fluctuations may originate from insufficient laser operation by the laser drivers, periodic vibrations of pumps turned on and off in the water plant, or other factors remaining unclear.

The absorbance for the single-ended detector signals was calculated to assess the long-term stability by

$$A = \log\left(\frac{I_0}{I_{(t)}}\right) \quad (5)$$

I_0 being the intensity at the initial measurement point of the long-term observation of the water-filled cell. This signal was used as a background for several hours of measurement time of the laser intensity $I_{(t)}$. Ideally, with no occurring changes of the measurement solution, this approach should yield an absorbance of 0. However, by employing this classic approach for process monitoring using a constant background spectrum for ATR spectroscopy, significant drifts over the course of several hours were observed (see Figure 4A,B). These drifts could be significantly reduced by exploiting the differently polarized laser beams for polarimetric-based balanced detection by

$$A_{pol.bal.} = \log\left(\frac{I_{mix(t)}}{I_{\parallel(t)}}\right) \quad (6)$$

https://dx.doi.org/10.1021/acssensors.0c01342
ACS Sens. 2021, 6, 35−42

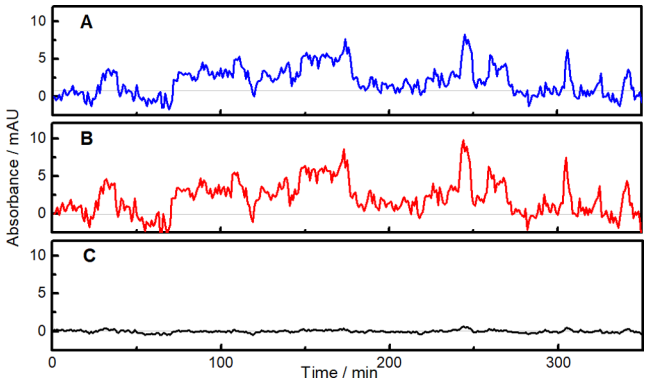

Figure 4. Absorbance of the water-filled cell over time in respect to a zero-line (gray dotted line). Absorbance obtained by the (A) mixed-polarized signal and the (B) parallel-polarized signal using the initial measurement point as a background. (C) Absorbance obtained via polarimetric balanced detection.

where $I_{\mathrm{mix}(t)}$ and $I_{\mathrm{II}(t)}$ are the simultaneously recorded intensities of the mixed-polarized beam and p-polarized beam, respectively (see Figure 4C). As mentioned before, the fluctuations of the channels scale with their absolute intensities (see Figure 3B), hence different signal heights were also taken into account for eq 6. Therefore, the intensity inserted into eq 6 for the mixed-polarized channels was divided by 7.81. This factor was obtained from the ratio between the intensity of the mixed-polarized channel divided by the p-polarized channel intensity. The use of the mixed-polarized beam with a lower effective thickness (see eq 2) as a reference and the p-polarized beam with a higher effective thickness (see eq 3) for sampling leads to enhanced long-term signal stability because background and sample spectra are recorded simultaneously (see Figure 4C).

Sensing Performance of Polarimetric Balanced Detection. To demonstrate the capabilities of the presented polarimetric balanced detection approach for process monitoring via ATR spectroscopy, ethanol in water was measured as a matching analyte for the emission characteristics of the employed QCL-XT.

The band height of the CH_2 twisting vibration (1273.5 cm^{-1}) from ethanol was used as an analytical signal for further investigations of the performance of the sensor. This band is obscured by the broad in-plane OH deformation vibration (1260−1400 cm^{-1}),[40] thus, a two-point baseline correction was applied to the recorded spectra using 1289.68 and 1265.43 cm^{-1} to determine the linear baseline. Here, the QCL-XT proved to be superior to classic DFB-QCLs as this procedure was only feasible due to the broad tuning capabilities of this novel laser type. In addition, unused spectral information for data interpretation was used as an inherent stability control of the system (see Figure 5). More spectral information would be obtainable via QCL-XT using additional laser lines. To evaluate the sensor performance, solutions containing 6, 8, 10, 20, and 30%$_{vol}$ ethanol were pumped through the sensor in an automated way by the employed sequential injection system.

First, the cell was filled with water and the intensity (I_0) was recorded, and then the ethanol solutions were injected into the cell starting with the lowest concentration and again the intensities ($I_{(t)}$) were recorded for the mixed- and p-polarized channel simultaneously. Every concentration was measured three times. First, the absorption for the mixed-and p-polarized

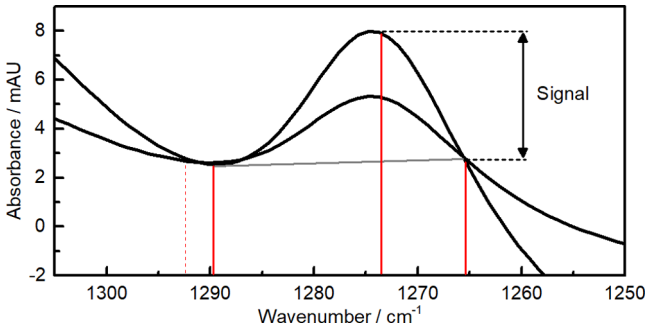

Figure 5. FT-IR spectra (solid black lines) of different concentrations of ethanol (25 and 50%$_{vol}$) in water. Wavenumbers emitted by QCL-XT used for spectra evaluation (solid red line) and as an inherent stability control (red dashed line), baseline correction (gray line) is enabled via the wide tunability of the QCL-XT.

channels as well as for the polarimetric balanced signal was obtained using eqs 5 and 6, respectively. Afterward, baseline correction via linear approximation (see Figure 5) was performed, yielding the final absorption for the mixed- and p-polarized channels as well as for polarimetric balanced detection. As depicted in Figure 6, the absorbance values

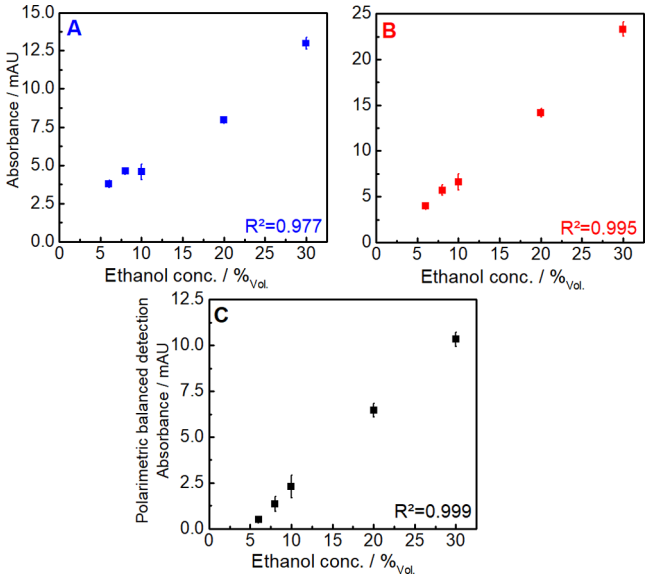

Figure 6. Sensor response to different concentrations of ethanol in water. Classic absorbance obtained via the signal from the (A) mixed-polarized and (B) parallel-polarized beams. (C) Absorbance calculated using polarimetric balanced detection.

obtained by the single-ended detector channels are different. Due to its higher effective thickness, the purely p-polarized beam yields higher absorbance values than perpendicular- or mixed-polarized beams (see eq 3 and Figure 6). Thus, for single-channel measurements, the purely p-polarized beam would be the preferred candidate for process monitoring via ATR spectroscopy in a low-noise environment.

Comparison of the analytical signals of the single-ended detector channels and the polarimetric balanced approach obtained via eqs 5 and 6 shows that the linear response of the sensor is enhanced via polarimetric balanced detection (see Figure 6). The low robustness of the mixed-polarized channel is made apparent by the high relative variance of the repetitions compared to the analytical signal. Both single-

https://dx.doi.org/10.1021/acssensors.0c01342
ACS Sens. 2021, 6, 35−42

ended channels exhibit the same relative standard deviation of approximately 3%. However, the smaller absorbance of the mixed-polarized channel as a consequence of the smaller effective thickness (see eq 2) is more susceptible to fluctuations than the p-polarized channel. The latter yields a higher measured absorbance corresponding to the higher effective thickness (see eq 3), thus leading to an improved sensing performance.

Evaluating the long-term experiment (Figures 3 and 4), it was found that polarimetric balanced detection increases long-term stability, hence the signal shows a root-mean-square (RMS) noise of 0.18 mAU over the whole experimental duration of almost 6 h (see Figure 4C). In contrast, the RMS noise of the p- and mixed-polarized channels as used for a classic absorbance-based ATR process analytical scheme with a constant background was found to be 2.2 and 1.9 mAU, respectively (see Figure 4A,B). Therefore, by employing polarimetric balanced detection, recording background, and sample spectra simultaneously, the long-term drift of the sensor could be decreased by a factor of 10 compared to single-ended detection conventionally employed in ATR process monitoring. The improvement of sensor stability via polarimetric balanced detection can be explained by eliminating external interferences. Similar to classic balanced detection schemes, where an extra reference channel for noise suppression is measured,[33] polarimetric balanced detection decreases noise by simultaneously measuring background and sample spectra but additionally allowing for long-term drift reduction due to real-time referencing.

Figure 6 shows that by polarimetric balanced detection, lower absorbance values are obtained than for the single-channel measurements. The absorbance obtained via polarimetric balanced detection (30%$_{vol}$ EtOH, 10.3 mAU) amounts exactly to the difference of the mixed- (13 mAU) and p-polarized (23.3 mAU) channels. This originates from the usage of the mixed-polarized channel as a reference and can be explained by

$$A_{\text{pol.bal.}} = \log\left(\frac{I_{\text{mix}(t)}}{I_{\parallel(t)}}\right) = \log\left(\frac{I_\sigma e^{-\varepsilon\, c\, d_{\text{e,mix}}}}{I_\sigma e^{-\varepsilon\, c\, d_{\text{e},\parallel}}}\right) \tag{7}$$

$$A_{\text{pol.bal.}} = \varepsilon\, c(d_{\text{e},\parallel} - d_{\text{e,mix}}) \tag{8}$$

where I_σ is the initial beam intensity influenced by common mode noise, ε is the absorption coefficient, c is the concentration of ethanol, and $d_{\text{e},\parallel}$ and $d_{\text{e,mix}}$ are the effective thickness experienced by the p- and mixed-polarized beam, respectively. Equation 7 illustrates that the common mode noise associated with I_σ is canceled out (see Figure 4) besides making background measurements (I_0) obsolete (compare eqs 5 and 8).

Finally, for performance comparison of the shown polarimetric balancing approach with classic ATR IR spectroscopy, the limit of detection (LOD) for polarimetric balanced detection and the mixed-polarized and p-polarized channel was calculated using

$$\text{LOD} = \frac{3 \times S_{\text{blank}}}{\text{slope of the calibration function}} \tag{9}$$

where S_{blank} is the standard deviation of five consecutive measurements of the water-filled cell. This resulted in an LOD of 3.77 and 2.85%$_{vol}$ for using the mixed- and parallel-polarized beams, respectively, as well as an LOD of 0.53%$_{vol}$ for polarimetric balanced detection. The standard deviation of the blank found for polarimetric balanced detection highlights the noise-canceling capabilities of this method, as it is significantly lower than for the other two channels (see Table 2).

Table 2. Quantitative Performance Parameters for Mixed-Polarized and p-Polarized Laser Beams and Polarimetric Balanced Detection

	mixed-polarized	p-polarized	polarimetric balanced
S_{blank} [mAU]	0.473	0.757	0.073
slope [mAU EtOH%$_{vol}^{-1}$]	0.376	0.795	0.410
LOD [EtOH%$_{vol}$]	3.77	2.85	0.53

The absorbance obtained via polarimetric balanced detection scales with the difference of the effective thicknesses of the p- and mixed-polarized channel (see eq 8), which is reflected by a lower slope of the calibration function. For the calculation of the LOD, the lower slope, however, is countered by the relatively higher reduction in noise (see Table 2). This resulted in an improvement of the LOD via polarimetric balanced detection by a factor of 5 compared to the p-polarized beam for classic ATR IR spectroscopy.

Equation 8 indicates that the introduced polarimetric balanced detection approach holds the potential to further increase the LOD by employing purely parallel- and perpendicular-polarized laser beams. This would result in a maximum obtainable difference of the effective thickness of 17.66 μm (see eqs 3, 4, and 8). However, the absorbance values in Figure 6C indicate that the effective thickness achieved by polarimetric balanced detection in the present setup is only 11.65 μm. This is linked to the usage of the mixed-polarized channel as a reference mostly composed of perpendicular-polarized light but also containing p-polarized light. Therefore, the higher differential effective thickness obtainable with purely polarized beams, yielding a higher absorbance, results in a higher slope and consequently further improvement of the LOD.

CONCLUSIONS AND OUTLOOK

This work introduces polarimetric balanced detection as a novel mid-IR ATR sensing scheme for liquids, exploiting the varying effective thicknesses of differently polarized laser beams for noise reduction and enhanced long-term stability. In the presented setup, employing a QCL-XT as a widely tunable mid-IR source, the laser emission is split into p-polarized and mixed-polarized beams via a ZnSe prism and guided toward a balanced thermoelectrically cooled MCT module. The developed mid-IR sensing device proved to provide robust results even during harsh conditions faced in on-site measurements. We took advantage of polarimetric balanced detection demonstrating the capabilities of this technique to reduce noise and long-term drifts besides obtaining quantitative information. Showcased by the measurement of different amounts of ethanol in water, polarimetric balanced detection outperformed single-ended detection, as the stability and the limit of detection of the sensor was improved. These findings demonstrate that polarimetric balanced detection is advantageous for chemical sensing via ATR spectroscopy and other applications, where long-term drifts are expected like in process analytical settings.

https://dx.doi.org/10.1021/acssensors.0c01342
ACS Sens. 2021, 6, 35−42

With this new ATR spectroscopy approach, classic background measurements prior to sample spectra acquisition become needless as the optical channel with the lower effective thickness serves as a reference signal recorded simultaneously with the channel providing a higher effective thickness used as a sample signal. Compared to setups where a reference beam is separated from the initial laser beam before sample interaction, our approach has the advantage to counter interference until the splitting of polarization,[32] therefore covering almost the complete beam path including sample interaction. In addition, polarimetric balanced detection enables simultaneous referencing, hence providing more analytical information with the same instrumental effort, as both balancing methods need one optical component to split the laser beam (prism or beam splitter[32]) and two detector elements. A more sophisticated approach for balanced detection uses an additional reference cell to probe the sample matrix.[41] Polarimetric balanced detection, however, only needs one probing interface for both background and sample measurement, hence also accounting for matrix effects using a simpler experimental manifold by taking advantage of ATR. We demonstrated that high initial noise levels of the employed mid-IR lasers and electronics can be reduced significantly by the presented approach. In the current design, polarimetric balancing attenuates noise in all parts of the beam path that is traversed by perpendicular- and p-polarized light together, including sampling; however, past the ZnSe prism, mechanical and thermal influences on the beam pointing introduce noise that may not be corrected.

In this work, a ZnSe prism was chosen as a polarizer, leading to incomplete separation of perpendicular- and parallel-polarized light resulting in a mixed-polarized beam. This design decision was made due to the broad mid-IR transparency of ZnSe; however, for a narrower wavelength range, alternative solutions, such as a MgF_2 Wollaston prism, could be used to completely separate perpendicular and parallel polarization and thus improve linearity for highly absorbing samples besides increasing the LOD.

QCL-XTs were shown to be an attractive alternative to EC-QCLs for broad band liquid-phase analysis, as they can be specifically tailored to the analytical needs and have the small instrument footprint of a housed DFB-QCL without any moving parts.[23] The monolithic character of QCL-XTs and the possibility to combine entire spectrometers on a chip suggest further integration into small lab-on-a-chip sensing devices.[42] Thus, further efforts may aim at miniaturization of the sensor, using functionalized ATR elements[5] and exploiting polarization-dependent absorption anisotropy for single-shot material characterization sensing schemes for mid-IR ATR spectroscopy.[43]

AUTHOR INFORMATION

Corresponding Author

Bernhard Lendl − *Institute of Chemical Technologies and Analytics, Technische Universität Wien, 1060 Vienna, Austria;* orcid.org/0000-0003-3838-5842; Email: bernhard.lendl@tuwien.ac.at

Authors

Stephan Freitag − *Institute of Chemical Technologies and Analytics, Technische Universität Wien, 1060 Vienna, Austria;* orcid.org/0000-0003-0179-2217

Matthias Baer − *Institute of Microwaves and Photonics, Friedrich-Alexander-University Erlangen-Nuremberg, 91058 Erlangen, Germany*

Laura Buntzoll − *Institute of Microwaves and Photonics, Friedrich-Alexander-University Erlangen-Nuremberg, 91058 Erlangen, Germany*

Georg Ramer − *Institute of Chemical Technologies and Analytics, Technische Universität Wien, 1060 Vienna, Austria;* orcid.org/0000-0001-8307-5435

Andreas Schwaighofer − *Institute of Chemical Technologies and Analytics, Technische Universität Wien, 1060 Vienna, Austria;* orcid.org/0000-0003-2714-7056

Bernhard Schmauss − *Institute of Microwaves and Photonics, Friedrich-Alexander-University Erlangen-Nuremberg, 91058 Erlangen, Germany*

Complete contact information is available at: https://pubs.acs.org/10.1021/acssensors.0c01342

Author Contributions

[§]S.F. and M.B. contributed equally to this work. All authors have given approval to the final version of the manuscript.

Notes

The authors declare no competing financial interest.

ACKNOWLEDGMENTS

Iren S.p.A, especially Nicola Bazzurro is acknowledged for granting access to the water treatment plant in Prato, Genova. This work received funding from the European Union's Horizon 2020 research and the innovation programme through the project WaterSpy and Hydroptics under grant agreement nos. 731778 and 871529. The authors acknowledge the TU Wien University Library for financial support through its Open Access Funding Program.

REFERENCES

(1) Griffiths, P. R.; De Haseth, J. A. *Fourier Transform Infrared Spectrometry*; John Wiley & Sons Ltd: Hoboken, New Jersey, 2007; Vol. *171*.

(2) Yoo, K. M.; Midkiff, J.; Rostamian, A.; Chung, C.-J.; Dalir, H.; Chen, R. T. InGaAs Membrane Waveguide: A Promising Platform for Monolithic Integrated Mid-Infrared Optical Gas Sensor. *ACS Sens.* **2020**, *5*, 861−869.

(3) Genner, A.; Martín-Mateos, P.; Moser, H.; Lendl, B. A. Quantum Cascade Laser-Based Multi-Gas Sensor for Ambient Air Monitoring. *Sensors* **2020**, *20*, 1850.

(4) Gasser, C.; Kilgus, J.; Harasek, M.; Lendl, B.; Brandstetter, M. Enhanced mid-infrared multi-bounce ATR spectroscopy for online detection of hydrogen peroxide using a supercontinuum laser. *Opt. Express* **2018**, *26*, 12169−12179.

(5) Baumgartner, B.; Freitag, S.; Gasser, C.; Lendl, B. A. Pocket-Sized 3D-printed Attenuated Total Reflection-Infrared Filtometer combined with Functionalized Silica Films for Nitrate Sensing in Water. *Sens. Actuators, B* **2020**, No. 127847.

(6) Koch, C.; Posch, A. E.; Herwig, C.; Lendl, B. Comparison of Fiber Optic and Conduit Attenuated Total Reflection (ATR) Fourier Transform Infrared (FT-IR) Setup for In-Line Fermentation Monitoring. *Appl. Spectrosc.* **2016**, *70*, 1965−1973.

(7) Crocombe, R. A. Portable spectroscopy. *Appl. Spectrosc.* **2018**, *72*, 1701−1751.

(8) Ramer, G.; Lendl, B. *Encyclopedia of Analytical Chemistry*; John Wiley & Sons, Ltd.: Hoboken, New Jersey, 2013.

(9) El Khoury, Y.; Collongues, N.; De Sèze, J.; Gulsari, V.; Patte-Mensah, C.; Marcou, G.; Varneck, A.; Mensah-Nyagan, A. G.; Hellwig, P. Serum-based differentiation between Multiple Sclerosis

and Amyotrophic Lateral Sclerosis by Random Forest classification of FTIR spectra. *Analyst* **2019**, 4647−4652.
(10) Haselmann, G. M.; Baumgartner, B.; Wang, J.; Wieland, K.; Gupta, T.; Herzig, C.; Limbeck, A.; Lendl, B.; Eder, D. In Situ Pt Photodeposition and Methanol Photooxidation on Pt/TiO2: Pt-Loading-Dependent Photocatalytic Reaction Pathways Studied by Liquid-Phase Infrared Spectroscopy. *ACS Catal.* **2020**, *10*, 2964−2977.
(11) Takamura, A.; Halamkova, L.; Ozawa, T.; Lednev, I. K. Phenotype Profiling for Forensic Purposes: Determining Donor Sex based on Fourier Transform Infrared Spectroscopy of Urine Traces. *Anal. Chem.* **2019**, 6288−6295.
(12) Comnea-Stancu, I. R.; Wieland, K.; Ramer, G.; Schwaighofer, A.; Lendl, B. On the identification of rayon/viscose as a major fraction of microplastics in the marine environment: discrimination between natural and manmade cellulosic fibers using Fourier transform infrared spectroscopy. *Appl. Spectrosc.* **2017**, *71*, 939−950.
(13) Schwaighofer, A.; Montemurro, M.; Freitag, S.; Kristament, C.; Culzoni, M. J.; Lendl, B. Beyond Fourier Transform Infrared Spectroscopy: External cavity quantum cascade laser-based mid-infrared transmission spectroscopy of proteins in the Amide I and Amide II Region. *Anal. Chem.* **2018**, *90*, 7072−7079.
(14) Lüdeke, S.; Pfeifer, M.; Fischer, P. Quantum-cascade laser-based vibrational circular dichroism. *J. Am. Chem. Soc.* **2011**, *133*, 5704−5707.
(15) Hinrichs, K.; Shaykhutdinov, T. Polarization-Dependent Atomic Force Microscopy−Infrared Spectroscopy (AFM-IR): Infrared Nanopolarimetric Analysis of Structure and Anisotropy of Thin Films and Surfaces. *Appl. Spectrosc.* **2018**, *72*, 817−832.
(16) Furchner, A.; Kratz, C.; Hinrichs, K. Sub-second infrared broadband-laser single-shot phase−amplitude polarimetry of thin films. *Opt. Lett.* **2019**, *44*, 4387−4390.
(17) Ebner, A.; Zimmerleiter, R.; Cobet, C.; Hingerl, K.; Brandstetter, M.; Kilgus, J. Sub-second quantum cascade laser based infrared spectroscopic ellipsometry. *Opt. Lett.* **2019**, *44*, 3426−3429.
(18) Alcaráz, M. R.; Schwaighofer, A.; Kristament, C.; Ramer, G.; Brandstetter, M.; Goicoechea, H. C.; Lendl, B. External-cavity quantum cascade laser spectroscopy for mid-IR transmission measurements of proteins in aqueous solution. *Anal. Chem.* **2015**, *87*, 6980−6987.
(19) Schwaighofer, A.; Alcaráz, M. R.; Araman, C.; Goicoechea, H.; Lendl, B. External cavity-quantum cascade laser infrared spectroscopy for secondary structure analysis of proteins at low concentrations. *Sci. Rep.* **2016**, *6*, No. 33556.
(20) Schwaighofer, A.; Lendl, B. *Vibrational Spectroscopy in Protein Research*; Elsevier: Cambridge, Massachusetts, 2020; pp 59−88.
(21) Schwaighofer, A.; Brandstetter, M.; Lendl, B. Quantum cascade lasers (QCLs) in biomedical spectroscopy. *Chem. Soc. Rev.* **2017**, *46*, 5903−5924.
(22) Li, J.; Chen, W.; Fischer, H. Quantum cascade laser spectrometry techniques: a new trend in atmospheric chemistry. *Appl. Spectrosc. Rev.* **2013**, *48*, 523−559.
(23) Villa, N.; Strübi, G.; Gresch, T.; Butet, J.; Blaser, S.; Müller, A. Quantum cascade lasers with discrete and non equidistant extended tuning tailored by simulated annealing. *Opt. Express* **2019**, *27*, 26701−26707.
(24) Bidaux, Y.; Bismuto, A.; Tardy, C.; Terazzi, R.; Gresch, T.; Blaser, S.; Muller, A.; Faist, J. Extended and quasi-continuous tuning of quantum cascade lasers using superstructure gratings and integrated heaters. *Appl. Phys. Lett.* **2015**, *107*, No. 221108.
(25) Slivken, S.; Bandyopadhyay, N.; Tsao, S.; Nida, S.; Bai, Y.; Lu, Q.; Razeghi, M. Sampled grating, distributed feedback quantum cascade lasers with broad tunability and continuous operation at room temperature. *Appl. Phys. Lett.* **2012**, *100*, No. 261112.
(26) Mittal, V.; Nedeljkovic, M.; Carpenter, L. G.; Khokhar, A. Z.; Chong, H. M.; Mashanovich, G. Z.; Bartlett, P. N.; Wilkinson, J. S. Waveguide Absorption Spectroscopy of Bovine Serum Albumin in the Mid-Infrared Fingerprint Region. *ACS Sens.* **2019**, *4*, 1749−1753.
(27) Jernelv, I. L.; Strøm, K.; Hjelme, D. R.; Aksnes, A. Infrared Spectroscopy with a Fiber-Coupled Quantum Cascade Laser for Attenuated Total Reflection Measurements Towards Biomedical Applications. *Sensors* **2019**, *19*, 5130.
(28) Haas, J.; Catalán, E. V.; Piron, P.; Karlsson, M.; Mizaikoff, B. Infrared spectroscopy based on broadly tunable quantum cascade lasers and polycrystalline diamond waveguides. *Analyst* **2018**, *143*, 5112−5119.
(29) Jernelv, I. L.; Høvik, J.; Hjelme, D. R.; Aksnes, A. *Biomedical Spectroscopy, Microscopy, and Imaging*; International Society for Optics and Photonics, 2020; p 113590A.
(30) Hobbs, P. C. Ultrasensitive laser measurements without tears. *Appl. Opt.* **1997**, *36*, 903−920.
(31) Waclawek, J. P.; Kristament, C.; Moser, H.; Lendl, B. Balanced-detection interferometric cavity-assisted photothermal spectroscopy. *Opt. Express* **2019**, *27*, 12183−12195.
(32) Kübel, J. M.; Botha, C.; Bucka, A.; Höpfner, J.; Zimmermann, H.; Godejohann, M.; Wilhelm, M. A. New Quantum Cascade IR-Laser Online Detector: Chemical-Sensitive Size-Exclusion Chromatography Measurement at Unprecedented Low Levels. *Macromol. Rapid Commun.* **2019**, *40*, No. 1900228.
(33) Akhgar, C. K.; Ramer, G.; Żbik, M.; Trajnerowicz, A.; Pawluczyk, J.; Schwaighofer, A.; Bernhard, L. The next Generation of IR Spectroscopy: EC-QCL based mid-IR Transmission Spectroscopy of Proteins with Balanced Detection. *Anal. Chem.* **2020**, *92*, 9901−9907.
(34) Doulamis, N.; Voulodimos, A.; Doulamis, A.; Bimpas, M.; Angeli, A.; Bakalos, N.; Giusti, A.; Philimis, P.; Varriale, A.; Ausili, A.; et al. WaterSpy: A High Sensitivity, Portable Photonic Device for Pervasive Water Quality Analysis. *Sensors* **2019**, *19*, 33.
(35) Baumgartner, B.; Freitag, S.; Lendl, B. 3D Printing for Low-Cost and Versatile Attenuated Total Reflection Infrared Spectroscopy. *Anal. Chem.* **2020**, *92*, 4736−4741.
(36) Freitag, S.; Baumgartner, B.; Tauber, S.; Gasser, C.; Radel, S.; Schwaighofer, A.; Lendl, B. An Acoustic Trap for Bead Injection Attenuated Total Reflection Infrared Spectroscopy. *Anal. Chem.* **2019**, *91*, 7672−7678.
(37) Milosevic, M. *Internal Reflection and ATR Spectroscopy*; John Wiley & Sons: Hoboken, New Jersey, 2012; Vol. *262*.
(38) Debenham, M. Refractive indices of zinc sulfide in the 0.405−13-μm wavelength range. *Appl. Opt.* **1984**, *23*, 2238−2239.
(39) Hale, G. M.; Querry, M. R. Optical constants of water in the 200-nm to 200-μm wavelength region. *Appl. Opt.* **1973**, *12*, 555−563.
(40) Socrates, G. *Infrared and Raman Characteristic Group Frequencies: Tables and Charts*; John Wiley & Sons: Hoboken, New Jersey, 2004.
(41) Akhgar, C. K.; Ramer, G.; Żbik, M.; Trajnerowicz, A.; Pawluczyk, J.; Schwaighofer, A.; Lendl, B. The Next Generation of IR Spectroscopy: EC-QCL-Based Mid-IR Transmission Spectroscopy of Proteins with Balanced Detection. *Anal. Chem.* **2020**, *92*, 9901−9907.
(42) Schwarz, B.; Reininger, P.; Detz, H.; Zederbauer, T.; Andrews, A. M.; Schrenk, W.; Strasser, G. Monolithically integrated mid-infrared quantum cascade laser and detector. *Sensors* **2013**, *13*, 2196−2205.
(43) Frogley, M. D.; Wang, C.; Cinque, G.; Barber, A. H. Polarised infrared microspectroscopy of edge-oriented graphene oxide papers. *Vib. Spectrosc.* **2014**, *75*, 178−183.